



HAL
open science

Faceting mechanisms of GaN nanopillar under KOH wet etching

Lucas Jaloustre, Saron Sales De Mello, Sébastien Labau, Camille Petit-Etienne, Erwine Pargon

► **To cite this version:**

Lucas Jaloustre, Saron Sales De Mello, Sébastien Labau, Camille Petit-Etienne, Erwine Pargon. Faceting mechanisms of GaN nanopillar under KOH wet etching. *Materials Science in Semiconductor Processing*, 2024, 173, pp.108095. 10.1016/j.mssp.2023.108095 . hal-04389931

HAL Id: hal-04389931

<https://hal.science/hal-04389931>

Submitted on 12 Jan 2024

HAL is a multi-disciplinary open access archive for the deposit and dissemination of scientific research documents, whether they are published or not. The documents may come from teaching and research institutions in France or abroad, or from public or private research centers.

L'archive ouverte pluridisciplinaire **HAL**, est destinée au dépôt et à la diffusion de documents scientifiques de niveau recherche, publiés ou non, émanant des établissements d'enseignement et de recherche français ou étrangers, des laboratoires publics ou privés.

Faceting mechanisms of GaN nanopillar under KOH wet etching

Jaloustre Lucas ^a, Sales De Mello Saron ^a, Labau Sébastien ^a, Petit-Etienne Camille ^a, Pargon Erwine ^{a*}

^a Univ. Grenoble Alpes, CNRS, CEA/LETI-Minatec, Grenoble INP, Institute of Engineering and Management University Grenoble Alpes, LTM, Grenoble F-38054, France

* erwine.pargon@cea.fr, Univ. Grenoble Alpes, CNRS, LTM, 17 rue des Martyrs, 38054 Cedex 09 Grenoble, France

Abstract

This study presents strategies for achieving GaN pillars with the desired *m*- (or even *a*-) oriented nonpolar facets through a top-down approach that combines plasma etching followed by room temperature KOH wet treatment processes. Indeed, GaN etching in KOH solution is an anisotropic process, meaning that it allows the appearance of stable facets at the macroscopic scale, while atomic processes, such as step-flow, drive the fundamental mechanisms of the wet etching at the microscopic scale. Our study highlights the key role played by both the shape (circular or hexagonal, aligned with either the *m*-planes or the *a*-planes) and the roughness of the hard mask in determining the resulting crystalline facet formation and their associated roughness. Furthermore, it underscores the importance of the GaN pillar profiles (reentrant, straight, tapered) after plasma patterning, as they strongly influence the subsequent wet etching mechanisms. Ultimately, the article demonstrates that smooth *m*-oriented facets can be achieved by using room temperature wet KOH (44 wt%) on slightly sloped GaN profiles after plasma etching, in conjunction with the use of hexagonal *m*-oriented hard masks.

Keywords: GaN, Plasma etching, Chemical etching, Faceting, step-flow process.

1. Introduction

Core-shell architecture presents a promising strategy for addressing the low efficiency of current planar III-N LEDs in the Ultra-Violet (UV) range [1,2]. This approach involves the fabrication of well-organized arrays of high aspect ratio ($AR > 10$) GaN nanowires, upon which the emissive quantum wells (QW) are radially grown. Typically, AlGaIn barrier/GaN QW structures are employed to achieve UV-A to UV-B emission (400-280 nm) [3–6]. The core-shell architecture offers several advantages, including reduced crystalline defects in the emissive layers, improved internal quantum efficiency through growth on GaN nonpolar crystalline planes (Quantum-confined Stark effect), increased emissive surface area, and enhanced light extraction [7,8]. Most research on GaN nanowires for UV emission has been carried out using a bottom-up approach based on Molecular Beam Epitaxy (MBE) [9] or Metal Organic Vapor Phase Epitaxy (MOVPE) [4–7]. However, controlling the dimensions and densities of the nanowires remains challenging with those approaches, as well as growing nanowires with diameter less than 1 μm .

Thus, the top-down approach, which combines lithography and plasma etching steps, shows significant promise as an industrial method for patterning arrays of high AR GaN nanopillars with controlled shapes, dimensions, and densities on a wafer scale. However, one challenge associated with the plasma patterning of GaN pillars is the potential for generating damaged and rough surfaces on the sidewalls, which may prevent from high-quality surface regrowth [10,11]. Moreover, the regrowth of the quantum wells on the nanowire sidewalls by MOVPE is favored if *m*-oriented nonpolar facets are present after the pillar patterning [4–7].

Our recent work demonstrates the considerable potential of a pure Chlorine plasma process for patterning anisotropic high AR GaN nanopillars. This process offers a reasonable etch rate (189 nm/min) and etch selectivity (13) over the SiO₂ hard mask (HM) [12]. However, our work also demonstrates that Cl₂ plasma leads to preferential crystal orientation etching in *a*-type facets, instead of the desired *m*-type facets if core shell application is targeted.

Due to the inability to obtain the m -oriented sidewalls through plasma etching alone, we investigate the capability of post-plasma etching wet KOH treatment. Indeed, several experimental studies [13–15] have observed that when GaN nonpolar a -plane $\{11-20\}$ and a -type semipolar plane $\{11-22\}$ surfaces are exposed to alkaline solutions, specific crystallographic m -type planes such as $\{10-10\}$ nonpolar planes, and $\{10-1-2\}$, $\{10-1-1\}$ semipolar planes, as well as c (0001) polar planes are revealed. The main reason is that wet KOH etching of GaN is an anisotropic process, meaning that it is slower along certain crystallographic directions than along others allowing the appearance of some stable facets [13,14,16–18]. The main mechanisms leading to such facets appearance at the macroscopic scale are driven by atomistic processes such as the step-flow process well described in references [19,20]. Step-flow process originates from the fact that the removal of the surface atoms is a site-dependent process at the microscopic scale. Each crystallographic plane present different atomic bonds configuration that has different energy barrier for the removal of the atom under a particular reactive environment and subsequently different reaction rates. The removal of these sites soon leads to the formation of steps that propagate along the plane and serve as a separation boundary between the lower and upper terraces.

In the case of GaN etching by KOH wet solution, the etching mechanism is based on the oxidation of gallium atoms through hydroxide (OH^-) molecules, which attack and break the Ga–N bonds, freeing the Ga atom to oxidize into Ga_2O_3 , which is subsequently dissolved in the solution [14,16,17]. Several authors have demonstrated that the etching ability of a plane strongly depends on planar densities and the number of negatively charged dangling bonds on the nitrogen atoms which repel OH^- [16–18]. Lai et al. [17] proposed a physical quantity called *etching barrier index* (EBI), which is the product of planar atom density and surface dangling bonds, to describe the etching resistivity of each GaN planes in an alkaline etching solution. The higher the EBI value of a plane is, the more difficult the etching of this plane would be. Based on this EBI index, semipolar planes ($\{11-2k\}$ and $\{1-10k\}$ with $k > 0$) etch faster than nonpolar ones ($\{11-20\}$ a -plane family and $\{1-100\}$ m -plane family) and faster than Ga (0001) c -polar planes. The increase stability of nonpolar planes compared to semipolar planes offers the possibility to reveal the desired m -facets if the wet KOH conditions are carefully controlled.

Thus, this article aims to provide strategies for achieving GaN pillars with the desired m -oriented nonpolar facets through a top-down approach that combines plasma etching with subsequent KOH wet treatment processes. After describing the methodology in section 2, section 3 focuses on the experimental wet KOH results applied after Cl_2 plasma etching of the GaN pillars. In this section, we emphasize the importance of retaining the SiO_2 HM during the KOH wet process to achieve an anisotropic transfer of the HM shape. Additionally, we highlight the critical role played by the GaN pillar profiles obtained through Cl_2 plasma etching prior to the wet KOH treatment. Furthermore, we note the significance of the HM shape (hexagonal shape with edges aligned with m - or a - GaN crystalline planes, or also circular) in determining the desired crystalline facet formation. Section 4 delves into the wet KOH etch mechanisms that explain the results of section 3. Finally, section 5 concludes by discussing how to fabricate m or a -oriented high aspect ratio GaN pillars by combining dry and wet etching techniques.

2. Experimental setup

2.1. Sample preparation

Micro-pillars fabrication was carried out on commercially available 4-inch wafer of unintentionally doped Ga-polar (0001) GaN of 4 μm thickness grown on c -sapphire substrate and provided by Nanowin company. From the datasheet specifications, the threading dislocation density is less than $5 \cdot 10^8 \text{ cm}^{-2}$. An 800 nm thick SiO_2 hard mask was deposited onto the GaN layer using Plasma Enhanced Chemical Vapor Deposition (PECVD) with tetraethoxysilane (TEOS) at 480 °C in a DxZ CVD reactor from Applied Materials.

The samples were then cleaned in acetone within an ultrasonic bath for 5 minutes at 45 °C, rinsed with isopropanol during 3 minutes, and dried with a nitrogen flow. Subsequently, an electron-sensitive resist (ma-N 2410) with a thickness of 800 nm was spin-coated on the samples using the following parameters: acceleration: 3500 rpm/s, speed: 2000 rpm, time 60 seconds. Finally, the resist curing was done by placing the samples on a hotplate set at 90 °C for 90 seconds.

The electron beam lithography (EBL) was then performed using a JBX-6300FS system from JEOL with an acceleration voltage of 100 kV, a current of 1 nA, and an exposure dose of 600 $\mu\text{C}/\text{cm}^2$. The resist development was done by submerging the sample into a MF26A developer during 90 seconds, followed by an immersion in a solution of MF26A and deionised water (volume ratio 1:9) during 30 seconds. The samples were then rinsed in deionised water during 8 minutes. The stack obtained after all these steps is shown on [Fig. 1-a](#).

The resist patterns consisted of dots with hexagonal or circular shapes, with diameters (inscribed circle) of 0.25 μm , 0.35 μm , 0.5 μm , 1 μm , and 2 μm . The hexagonal dots had two orientations corresponding to a -planes $\{11\bar{2}k\}$ and m -planes $\{10\bar{1}k\}$ of GaN, with a precision of $\pm 1^\circ$ (cf. [Fig. 1-b](#)). The dots follows a staggered arrangement with two different densities: A dense array with a distance between the dots of 2.5 μm and an isolated array with a distance between the dots of 5.5 μm (cf. [Fig. 1-c](#)). The primary focus in this work will be on the 0.5 μm diameter pillars within the isolated array, but the observed trends are consistent across different pitches and diameters.

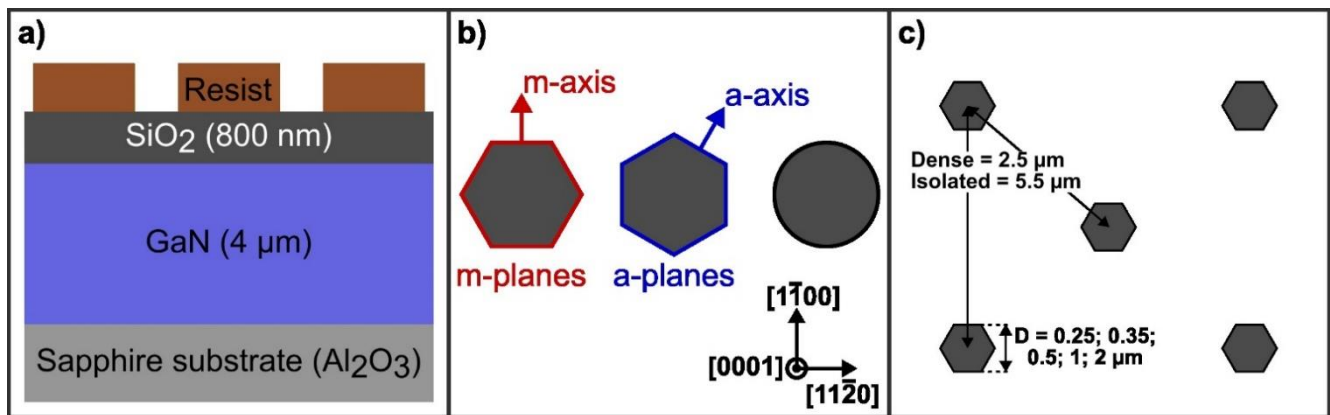


Figure 1. a) Schematic of the stack used, b) Shapes of the lithography dots, hexagonal oriented with a - or m - planes of the GaN or circular. c) Staggered arrangement of the dots with the annotations of dots diameters and distance between them for the two arrays.

2.2. Plasma and wet processes

The etching experiments were conducted using a Centura 5200 etch platform from Applied Materials, which consists of three plasma reactors designed for 200 mm wafers.

For the initial HM opening step, GaN samples were thermally glued onto a 200 mm SiO_2 carrier wafer (CW) using silicone-free thermal paste (Type 1977-DP) from Techspray. The SiO_2 hard mask was then etched with an $\text{Ar}/\text{C}_4\text{F}_8/\text{O}_2$ plasma in a Magnetically Enhanced Reactive Ion Etching (MERIE) reactor from Applied Materials. The etching parameters were as follows: a gas flow of 500 sccm for Ar, 20 sccm for C_4F_8 and 5 sccm for O_2 , an RF power of 1500 W, a magnetic field of 30 gauss, and a pressure of 50 mTorr. This plasma process ensured a SiO_2 /resist etch selectivity of 1.7 and a SiO_2 etching rate of 330 nm/min.

Subsequently, for both resist stripping and GaN etching steps, the samples were thermally glued on a 200 mm SiN carrier wafer, and the plasma processes were operated in an Inductively Coupled Plasma (ICP)

reactor (Decoupled Plasma Source, DPS, from Applied Materials). The resist was stripped using an O₂ plasma with an O₂ gas flow of 90 sccm, a source power of 800 W, no bias power (0 W), and a pressure of 10 mTorr. Finally, the GaN layer were etched with a Cl₂ plasma. In this study, parameters such as Cl₂ flow, source power and direct current voltage on the chuck (V_{DC}) were kept constant at 190 sccm, 400 W, and -450 V respectively. The variable adjusted during experimentation was the chamber pressure, which ranged from 15 mTorr to 30 mTorr to achieve precise control over the GaN pillar profiles. It is worth noting that in our tool, only bias power (Wb), not V_{DC}, could be adjusted. As pressure increased, the ion flux diminished, necessitating a decrease in bias power to maintain a constant V_{DC} while raising pressure. The bias power at different pressures varies as follows: 170 Wb at 15 mTorr, 150 Wb at 20 mTorr, 140 Wb at 25 mTorr and 135 Wb at 30 mTorr. The chuck temperature was maintained at 55 °C. The GaN etching process was monitored in real-time and stopped at the end of the process using an endpoint system (EyeD from Verity instrument) based on interferometry. Additional details on the experimental protocol can be found in reference [12].

The wet etching experiments were performed in a chemical fume hood located within a clean room, with the temperature maintained at 20 °C. To remove the SiO₂ hard mask after GaN etching, a buffered oxide etch (BOE) solution was employed. This commercial BOE solution provided by TECHNIC consisted of a 7:1 volume ratio of 40% NH₄F in water to 49% HF in water and was applied at room temperature for a duration of 2 hours. Subsequently, a 44 wt% KOH solution provided by CMC Materials was used at room temperature for the post-etching wet treatment. For both wet treatments, the samples were submerged into the solution with the patterned side facing upward, and without any agitation. Various KOH etching times were investigated, ranging from 3 hours to 48 hours, only the most noteworthy will be discussed. Following the wet treatments, the samples were rinsed in deionized water for 2 minutes and dried using a nitrogen (N₂) flow.

2.3. Morphological characterizations

A FEI Helios-450s Focused Ion Beam Scanning Transmission Electron Microscopy (FIB-STEM) system was used to image the pillars after the different steps of dry and wet etching. Observations were conducted at 3 kV and 50 pA to mitigate charging effects, and the samples were tilted by 45 ° to show pillar sidewalls.

3. Wet KOH results

KOH experiments were conducted following GaN etching in Cl₂ plasma at 25 mTorr. Under these plasma conditions, the pillar profiles were nearly anisotropic, featuring a slight bulge located 1 μm below the top (cf. [Fig. 2-a](#)). As explained in our previous study, this bulge corresponded to a Si-based passivation layer formed by the redeposition of SiN CW and GaN etch byproducts [12]. The passivation layer measured approximately 25 nm in thickness at the top of the pillar, reaching its maximum thickness of 55 nm at a depth of 1 μm below the top (in the bulge area). It then gradually thinned out and disappeared towards the base of the pillar. After BOE treatment (used to remove the HM), this passivation layer was removed, resulting in the GaN pillars displaying nearly perfect anisotropy (cf. [Fig. 2-d](#)). As also discussed in our previous study, it was observed that the GaN pillars after Cl₂ plasma etching presented facets oriented along the nonpolar *a*-plane (cf. [Fig. 2-d](#)) regardless of the HM shape.

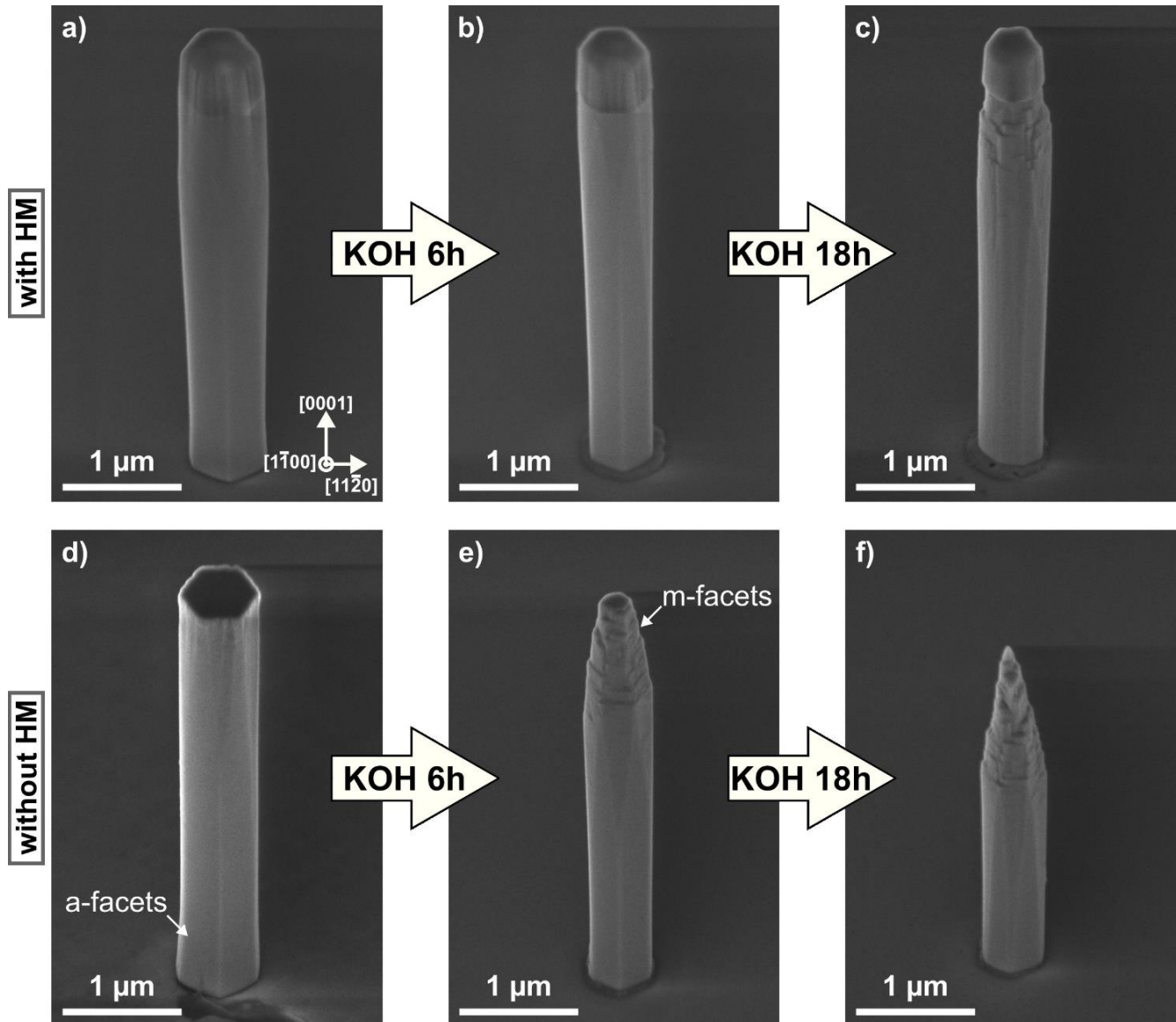


Figure 2. SEM images of 0.5 μm diameter GaN pillars patterned with *m*-oriented HM and Cl_2 plasma at 25 mTorr after KOH wet operated a)-c) with HM, d)-f) without HM. a) is the image after plasma etching and d) is the pillar after plasma etching and HM removal with BOE.

The GaN samples with and without the HM were then dipped in a KOH solution:

Without HM, the pillars experienced erosion at their uppermost part, and this degradation gradually extended both vertically and horizontally as the KOH duration increased, creating a rough staircase pattern profile (cf. [Fig. 2-e and 2-f](#)).

On the other side, the *a*-type nonpolar planes constituting the pillar sidewalls exhibited remarkable stability and remained relatively unetched even during extended KOH exposure (cf. [Fig. 2-f](#)). The GaN etching mechanism appeared to occur at the junction between the *c*- horizontal plane and the nonpolar vertical planes, propagating vertically and horizontally. It is worth mentioning that damage at the pillar's top induced the appearance of *m*-facets regardless of the initial HM shape (cf. [Fig. 3](#)).

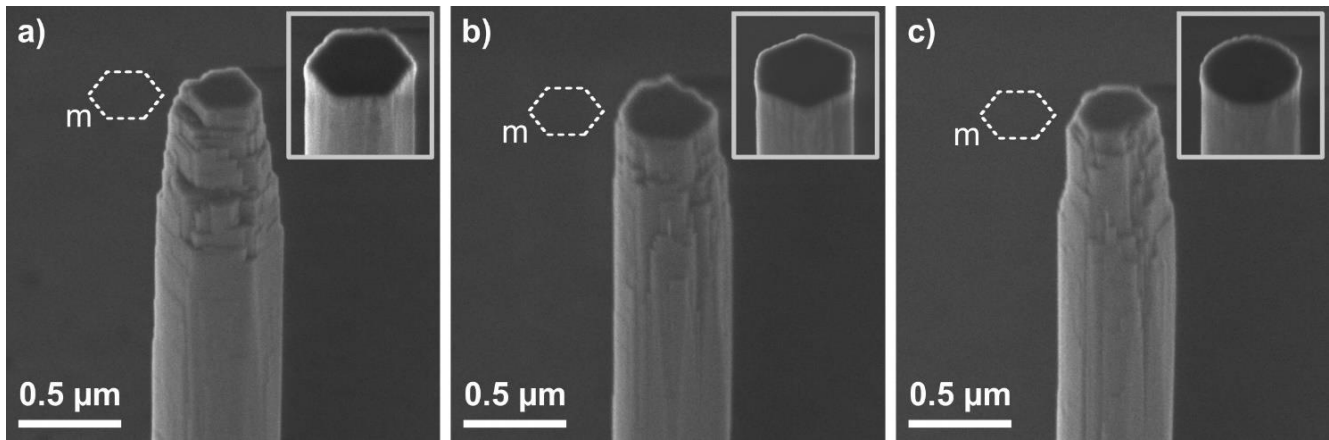


Figure 3. SEM images of 0.5 μm diameter GaN pillars without HM (removed by BOE) after 3 hours of KOH. The HM shape before BOE was: a) *m*-oriented, b) *a*-oriented, c) circular. The framed images in the top right corner corresponds to the pillars shape before KOH treatment.

When the HM was kept in place (cf. [Fig 2-a, 2-b, 2-c](#)), there was no consumption of the uppermost part of the pillar after 6 hours of KOH treatment. However, with longer KOH durations, degradations began to appear at the top. This degradation was explained by the slow lateral etching of the SiO_2 HM during the KOH wet (measured at around 3-3.5 nm/hour). Indeed, the lateral consumption of the HM slowly exposed the GaN, leading to similar wet etching mechanisms as those observed without HM. Aside from the top pillar erosion during extended KOH treatment, the GaN pillar dimension and profile did not evolve much with longer KOH exposure. The profile evolution between plasma etching and 6 hours KOH treatment was due to the removal of the SiO_x -based passivation layer by the KOH. However, as in the case without HM, the *a*-nonpolar planes present after plasma etching remained very stable with KOH treatment time.

This first experiment highlighted the crucial role of the HM presence to avoid the top pillar degradation, provided that KOH treatment time was not too long.

A second set of KOH experiments was performed on GaN pillars presenting various profiles after Cl_2 etching (cf. [Fig. 4](#)). The GaN profiles were obtained by changing the pressure while maintaining a constant V_{DC} to ensure similar ion energy for all investigated conditions.

By increasing the pressure from 15 mTorr to 30 mTorr, the GaN pillar profile transitioned from tapered to reentrant, as illustrated in [Fig. 4-a to 4-d](#) for a *m*-oriented HM. Comparable profiles were obtained with *a*-oriented or circular hard masks, as shown in our previous study [12].

Increasing the pressure enhanced the chemical component of the plasma etching, namely increasing the Cl radical flux over the ion flux. This resulted in a decrease in vertical etch rates from 248 nm/min to 121 nm/min when increasing the pressure from 15 mTorr to 30 mTorr. Concurrently, the lateral etch driven by Cl radicals was enhanced, allowing the profile control from tapered to reentrant.

It was also observed that increased pressure favored the formation of *a*-facets, consistently with preferential crystal orientation etching mechanisms involved in Cl_2 plasma and driven by the chemical aspect of the etching [12].

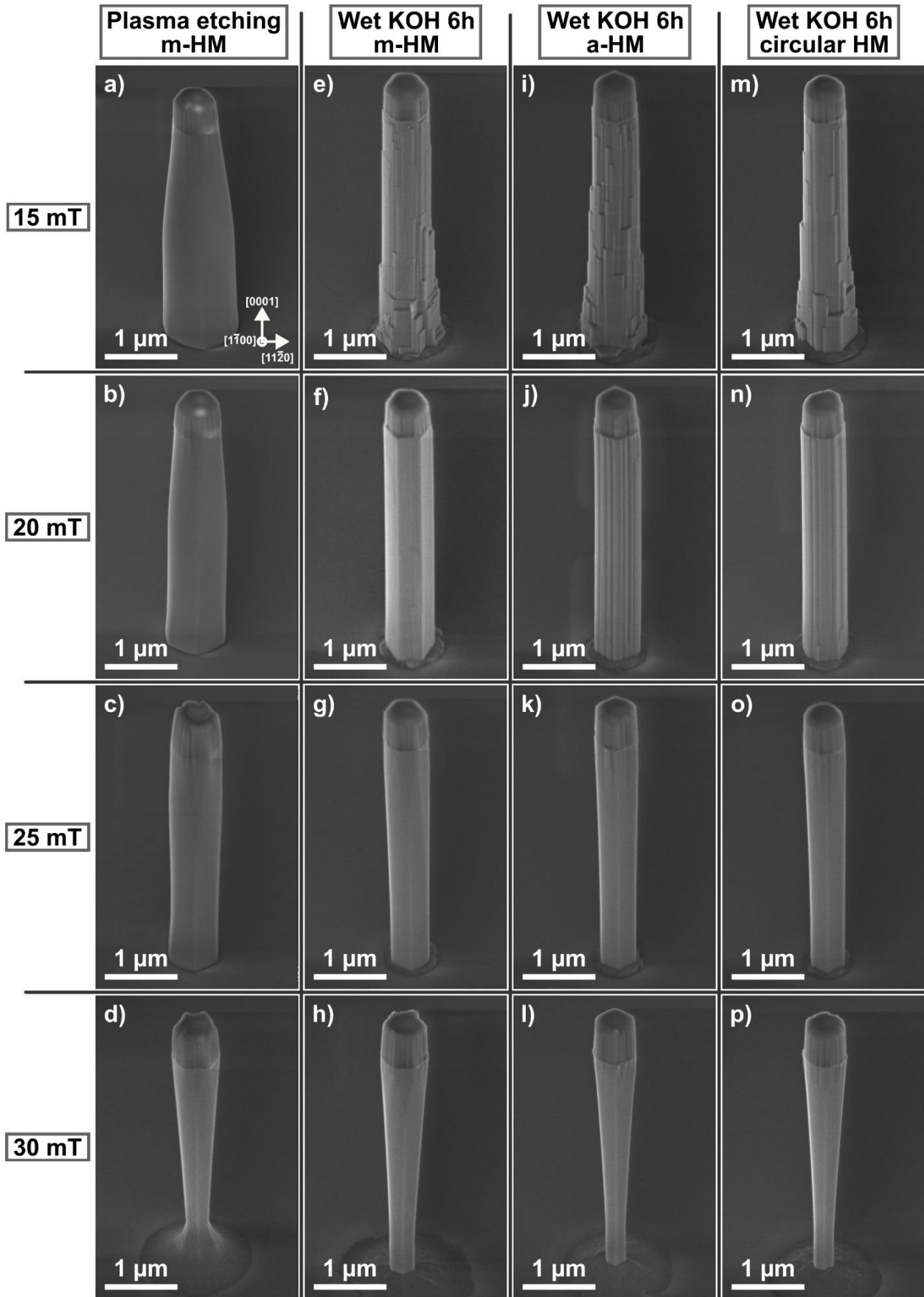


Figure 4. SEM images of 0.5 μm diameter GaN pillars: a), b), c), d), after plasma etching at 15, 20, 25, and 30 mTorr with m-oriented hard masks respectively. e)-p) after 6 hours KOH wet for m-oriented hard masks e)-h), for a-oriented hard masks i)-l), and for circular hard masks m)-p).

After Cl_2 etching using the various pressures, the GaN pillars with *m*-oriented, *a*-oriented, and circular HMs were immersed in the 44% KOH solution. Figure 4 highlights the influence of the GaN profile after plasma etching on the faceting effect. For reentrant (30 mTorr, Fig. 4-h, 4-l, 4-p) or anisotropic profiles (25 mTorr, Fig. 4-g, 4-k, 4-o), the wet etching had minimal impact, mostly removing the passivation layer. It should be noted that for the 30 mTorr conditions (and to a lesser extent 25 mTorr), the pillars exhibited some foot after plasma etching, which was completely removed by the wet KOH, straightening the pillar profile.

On the contrary, if the pattern exhibited a slight slope (20 mTorr, Fig. 4-f, 4-j, 4-n) or a strong slope (15 mTorr, Fig. 4-e, 4-i, 4-m), the wet etching progressed along the entire slope profile from the upper to the lower regions. This gradual progression resulted in the effective transfer of the hard mask shape into the pillar. In the case of a strong slope (15 mTorr), a 6-hour processing time of KOH was too short to remove the excess of GaN at the pillar's base, preventing the complete transfer of the hard mask dimensions. However, combining a slightly tapered GaN profile (20 mTorr) with a 6-hour KOH treatment allowed for precise transfer of the HM dimensions and shapes. This phenomenon was observed for all initial HM shapes. For extended KOH etching (24 hours and beyond), the protection provided by the HM was no longer sufficient, and damage began to appear, their propagation and characteristics were similar to the case where no HM was used, as visible in Fig 2-c. Another noteworthy observation was that when using an *m*-oriented HM, the pillars exhibited remarkably smooth and well-defined *m*-facets throughout the entire pattern height (cf. Fig. 4-f and Fig. 5-a). When using an *a*-oriented hard mask, the GaN sidewalls were aligned with *a*-planes but they presented distinct prism-like structures with multiple vertical zigzag lines. These vertical lines closely followed the striated HM sidewalls (cf. Fig. 4-j and Fig. 5-b). Note that the striations present on the HM sidewalls were not created by the KOH wet but were already present after GaN etching. They can be guessed in Fig. 4-a and Fig. 4-d, but are less visible because covered by the passivation layer formed during GaN plasma etching. These striations were formed during the hard mask opening step. The formation of striations in the hard mask during plasma etching transfer has been well documented experimentally [21,22] and by modelling [23,24]. It comes from the initial sidewalls roughness of the resist pattern after lithography. Due to the anisotropic nature of plasma etching because of the ion directionality, the shadowing of ions by the roughness features on the sidewall of the initial resist is found enough to induce striations at the sidewalls of the underlying substrate.

Finally, in the case of circular hard masks, the pillars' sidewalls displayed a combination of smooth *m*-facets and striated *a*-planes (cf. Fig. 4-n and Fig. 5-c).

These results highlight the necessity of sloped GaN profiles to achieve the desired transfer of the HM dimensions and shapes and to achieve the desired faceting.

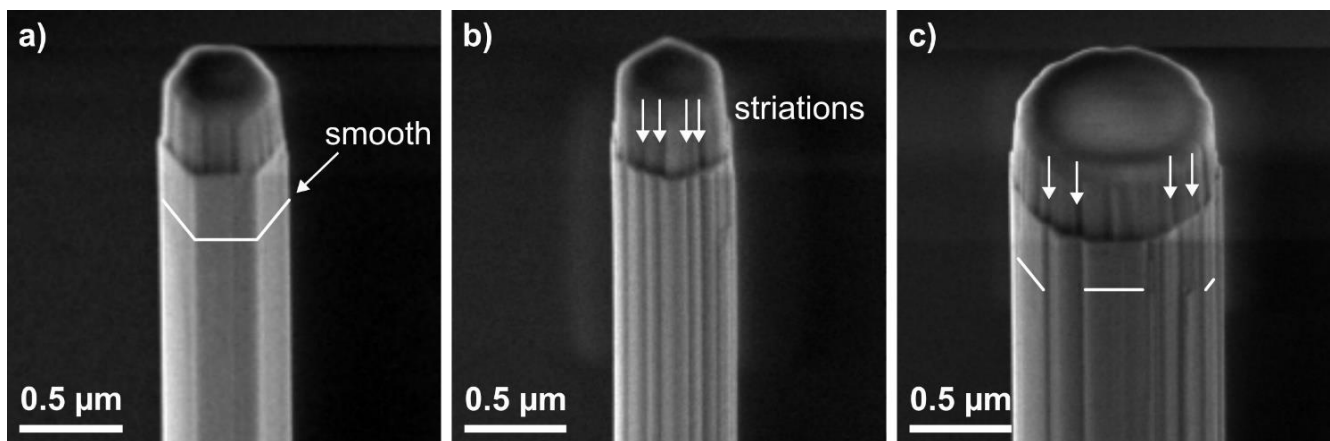


Figure 5. SEM images of pillars after plasma etching at 20 mTorr and KOH 6 hours on: a), b), 0.5 μm diameter pillars with *m*-oriented and *a*-oriented hard masks respectively (zoom images from Fig. 4-f and 4-j). c) 1 μm diameter pillar with a circular hard mask. The solid lines represent the *m*-planes, while the arrows indicate the striations of the hard mask transferred onto the sidewalls

It is noteworthy to mention that the results obtained in [Figure 4](#) are highly reproducible from sample to sample and within the same sample whatever the pillar density or diameter. For the process allowing the *m*-faceting appearance (the combination of Cl₂ etching at 20mT followed by 6-hour KOH, cf. [Fig. 4-f](#)) more than 10 samples have been produced with the same repeatability over the 500 000 pillars present on a single sample. [Figure 6](#) illustrates the reproducibility within one sample for the *m*-oriented hard mask according to the pillar density.

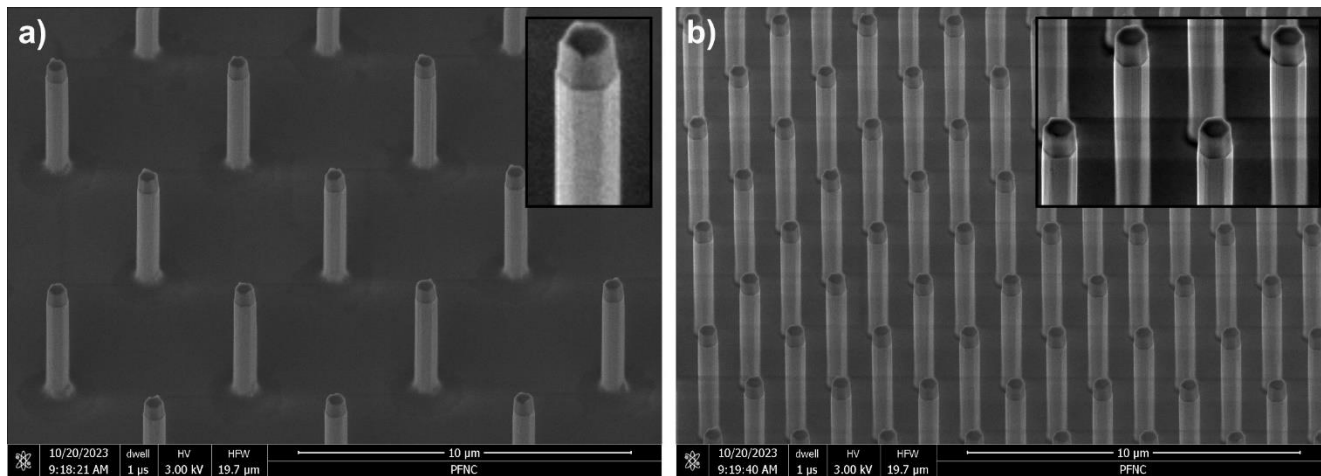


Figure 6. SEM images of 0.5 μm diameter pillars with *m*-oriented HM in a case of a) isolated array, b) dense array. The top right framed images corresponds to a zoomed image of a single pillar with enhanced brightness and contrast.

The results obtained in section 3 are discussed in the next section.

4. Discussion

If no hard mask is present, the free *c* Ga-polar plane at the top of the pillar acts as an etch-stop facet according to the EBI factor [17]. However, the top edges of the GaN pillar have been damaged by the previous plasma etching step, revealing some kink sites that are more vulnerable to the wet etching [18]. The removal of these sites soon leads to the formation of steps on both the *c*-horizontal and *a/m* vertical planes, creating some upper and lower passive terraces as described by the step-flow process concept [19]. Those steps propagate horizontally along the *c*-plane and vertically along the *a/m* plane through a mechanism referred as kink propagation. Each created step edge becomes vulnerable, leading to the formation of terraces that align with the most stable planes (cf. [Fig. 7-a](#)). In our case, these are the *c* and *m* planes, explaining the staircase like roughness observed in [Fig. 2-e, 2-f](#) and in [Fig 3](#). This propagation mechanism is depicted in [Fig. 8-b](#) and [Fig. 8-e](#).

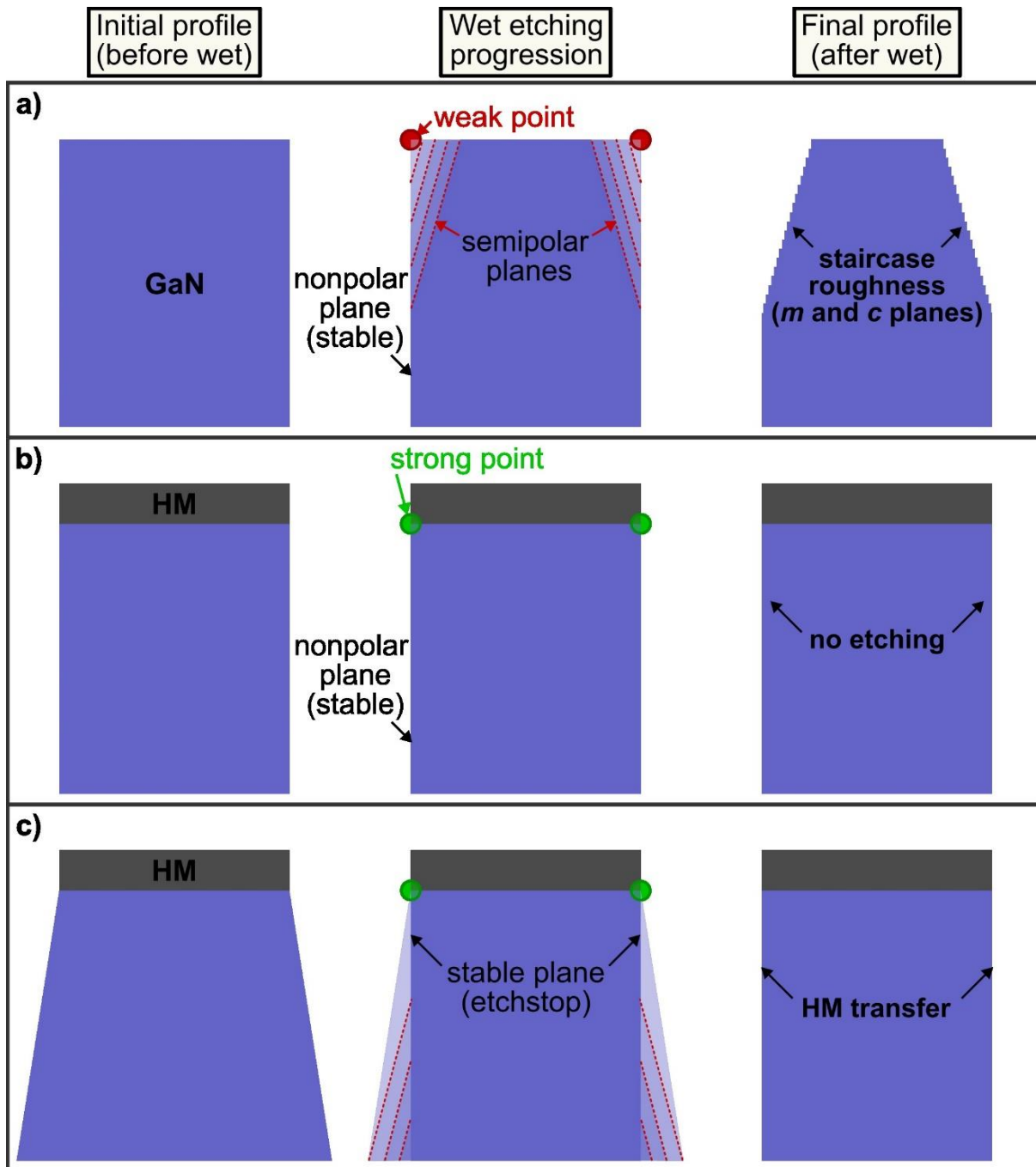


Figure 7. Schematic representation of GaN profile evolution during wet KOH in the case of a) pillars without HM, b) pillars with HM and with a straight profile, c) pillars with HM and with tapered profile. The red dashed lines indicate the progression of wet etching.

If the HM is in place (and not laterally consumed by the wet), the top edges of the pillars are protected from the wet etching. This means that etching will not be triggered at this weak location. In contrast, the wet etching will occur depending on the kink sites present on the pillar sidewalls after plasma etching patterning. When GaN pillars present smooth and vertical a -plane surfaces (25 mTorr or 30 mTorr cases), the pillar sidewalls are not etched by KOH (cf. Fig. 7-b). This confirms that the a -nonpolar planes obtained after plasma etching are defect-free and chemically stable under room temperature KOH used in this study. On the other hand, the foot of the pillars corresponding to a semipolar plane, is quickly etched until it reaches the more stable a -plane. Note that based on the angle of around 71° measured between the foot plane and the horizontal, could correspond to a $\{11\text{-}21\}$ semipolar plane.

When a slight (20 mTorr case) or a strong (15 mTorr case) slope is present, the tapered sidewalls which correspond to *a*-type semipolar planes are not protected by the HM and are attacked rapidly by the wet KOH. The etching proceeds along the normal of the semipolar plane, while revealing at the same time the *c* and *m* stable facets. The semipolar planes will quickly be transformed into a collection of {1-100} and {0001} terraces. However, the HM presence prevent further lateral expansion of the etching along the *c* plane at the top pillar edge, the semipolar planes are quickly transformed into stable vertical nonpolar *m*-planes on which the etching process stops (cf. [Fig. 7-c](#)). This explains the anisotropic profiles obtained after wet KOH and the transfer of the HM shape. From the atomistic point of view, He et al. [25] show that the etch stops when the whole *m*-plane sidewall surface ends up with N atoms having negatively charged dangling bonds.

On the other hand, one result of our study is inconsistent with the observations of some other works. In our study, the *a*-nonpolar plane sidewalls of the GaN pillar obtained after plasma etching remain laterally unetched and smooth during the KOH wet etching (cf. [Fig. 4-g, 4-h, 4-k, and 4-l](#)), while other studies show that this plane is etched with the appearance of *m*-type facets, roughening the surface [14,15,25,26]. In all the mentioned studies, the experimental conditions can be very different. Therefore, it is difficult to draw some clear conclusions. However, except for Itoh's work, the alkaline wet etching was conducted above room temperature (between 60 °C and 90 °C) [15,25,26]. We think that temperature plays a role in the activation of the etching of the *a*-plane, which may explain why in their case this plane is etched. A temperature increase allows to activate some sites on the *a*-plane and allows the unzipping process and finally reveal the most *m* stable planes. In Itoh's work [14], (where room temperature KOH is applied to patterned trenches with sidewalls aligned with the *a*-plane), we think that the appearance of rough *a*-plane sidewalls after KOH is due to the fact that after plasma patterning, they do not have perfectly smooth and vertical *a*-facets sidewalls, as it is the case for our pillars. Thus, their sidewalls after etching is more like a defective *a*-type semipolar plane surface that can be attacked by the wet.

By cross-referencing information from their publications, we think that *a*-nonpolar planes are chemically inert under room temperature alkaline wet etching providing no kink sites present, and that an increase of temperature helps to activate the etching of some sites.

The last result to explain is the presence of numerous striations on the pillar sidewalls when an *a*-oriented HM is used, which significantly differs from the very smooth sidewalls obtained with an *m*-oriented HM.

As discussed above, the etching of semipolar planes by an alkaline solution reveals preferentially *c* polar and *m*-nonpolar facets. If the etch is guided by the edge of an *m*-oriented HM, it will reveal several parallel *m*-nonpolar planes aligned with HM edges, resulting in the formation of staircase-like sidewalls composed of *c*- and *m*-planes (cf. [Fig. 8-a](#) and [Fig. 8-b](#)). The etch will stop when all the vulnerable step edges not protected by the hard mask are removed, and at this point only the smooth and stable *m*-facets aligned with the HM edges remains (cf. [Fig. 5-a](#) and [Fig. 8-c](#)).

If the etch is guided by the edge of an *a*-oriented HM, *m*-planes are also revealed by the wet KOH. However, to conform to the *a*-orientation of the HM, the sidewalls will transform into a collection of *m*-oriented triangular prism-like shapes, each with a 120 ° angle at the vertices of the triangles (cf. [Fig. 8-d](#) and [Fig. 8-e](#)).

This results in the emergence of vertical prism-shaped striations on the *a*-plane that propagates as indicated in [Fig. 8-e](#). Considering a top view of the pattern (cf. [Fig. 8-f](#)), when the successive *m*-oriented triangles reach the striated HM edges (that block the lateral progression), they will fit in the shape of the HM striated roughness while maintaining their *m*-oriented edges. It gives the impression that the HM striations are transferred into the GaN sidewalls but the morphology of the striations are not exactly the same (cf. [Fig. 5-b](#) and [Fig. 8-f](#)).

If the initial HM shape is circular, the final sidewalls will be a mixed of smooth *m*-planes and striated *a*-planes surfaces (cf. [Fig. 5-c](#)).

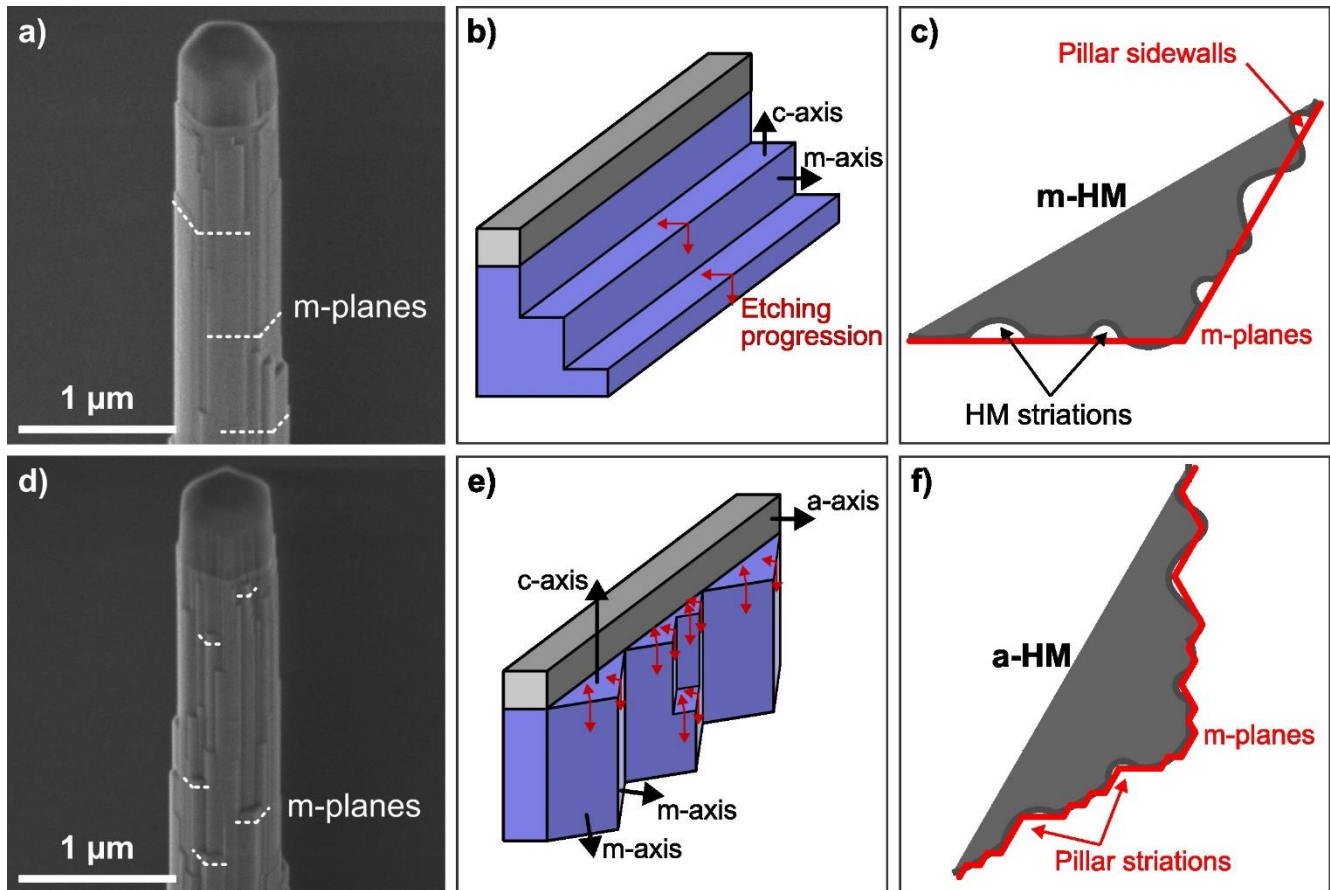


Figure 8. a), d) SEM images of pillars after partial KOH etching (15 mTorr, 6 hours KOH) for *m*-oriented and *a*-oriented hard masks, respectively. b), e) Schematic representations illustrate facets formation and etching propagation in the case of *m*-oriented and *a*-oriented hard masks, respectively. The red arrows show the step edge propagation. c), f) Schematic representations illustrate the impact of hard mask striations on the pillar sidewalls in the case of *m*-oriented and *a*-oriented hard masks, respectively.

5. Conclusion

The ability to pattern GaN features with anisotropic and smooth crystalline facets is of great interest for many optoelectronics applications including core shell UV LEDs. In this article, we provide strategies to obtain anisotropic GaN pillars with the desired *m*- (or even *a*-) oriented nonpolar facets through a top-down approach that combines Cl_2 plasma etching followed by KOH wet processes. Our study reveals that three main factors may influence the final GaN pillar profile after wet etching. First, the presence of the HM during the wet prevents the degradation of the pillar top and allows the anisotropic transfer of the HM dimension and shape. Secondly, the GaN pillar profiles after plasma etching drive the subsequent KOH wet etching mechanism. Indeed, our study shows that vertical *m* and *a* nonpolar planes, as well as horizontal *c* planes, are chemically inert to room temperature KOH if no kink sites are present. On the contrary, oblique semipolar planes are etched, and the etch propagates along the normal of the semipolar planes by revealing *m*-type and *c* facets. Consequently, if before wet etching the GaN pillars present smooth and vertical nonpolar plane surfaces well-aligned with the HM edge, the pillars will not be etched by KOH. However, if a slope is present, the tapered sidewalls corresponding to *a*-type semipolar planes are etched rapidly by the wet KOH. The etching proceeds along the normal of the semipolar plane, while revealing at the same time the *c* and *m* stable facets. The semipolar planes are quickly transformed into a collection of $\{1-100\}$ and $\{0001\}$ terraces, the most stable planes. The etch stops once the lateral extension of the etching, blocked by the presence of the hard mask is not possible anymore.

Finally, the HM shape (hexagonal or circular) drives the formation of the crystalline facets. If the HM is m -oriented, the wet etch proceeds through the formation of both m -planes aligned with the HM edges and c planes creating a staircase like roughness. Once the vertical m -plane below the HM edge is reached, the etch stops on smooth m -vertical facets. On the other hand, if an a -oriented HM is used, similar etch mechanisms are in place but the wet etch must adapt to the fact that the etch is guided by an a -oriented hard mask. The consequence is that the GaN sidewalls will transform into a collection of m -oriented triangular prism-like shapes, each with a 120° angle at the vertices of the triangles. These shapes will conform to the striations present on the HM, ultimately resulting in rough, striated a -facet sidewalls.

Based on these observations, if GaN pillars with smooth m -oriented facets are desired, they can be obtained by combining a slightly sloped GaN profile after Cl_2 etching with the use of a hexagonal m -oriented hard mask followed by a 44% wet KOH process (6-hour in our case). A similar approach can be used to obtain a -oriented GaN pillars, but in this case, the facets will be composed of rough vertical prism-shaped striations with m -planes. Therefore, to get GaN pillars with smooth a -oriented facets, we recommend to transfer into the GaN layer an a -oriented hexagonal hard mask with Cl_2 plasma etching process with the adapted plasma conditions (e.g. 25 mTorr in our study that leads to anisotropic GaN profiles). After HM and passivation layer removal, anisotropic GaN pillars with smooth a -facets can be obtained as shown in our previous study [12].

Acknowledgement

This research was funded by the French National Research Agency in the framework of the program ANR-22-CE51-0032-01 and the French National Research Agency in the framework of the "Investissements d'avenir" program (ANR-15-IDEX-02). It was also supported by the French RENATECH network.

- [1] Y. Ra, S. Kang, C. Lee, Ultraviolet Light- Emitting Diode Using Nonpolar AlGa_N Core–Shell Nanowire Heterostructures, *Advanced Optical Materials*. 6 (2018) 1701391. <https://doi.org/10.1002/adom.201701391>.
- [2] Y. Zhao, H. Fu, G.T. Wang, S. Nakamura, Toward ultimate efficiency: progress and prospects on planar and 3D nanostructured nonpolar and semipolar InGa_N light-emitting diodes, *Adv. Opt. Photon*. 10 (2018) 246–308. <https://doi.org/10.1364/AOP.10.000246>.
- [3] R. Koester, J.-S. Hwang, D. Salomon, X. Chen, C. Bougerol, J.-P. Barnes, D.L.S. Dang, L. Rigutti, A. de Luna Bugallo, G. Jacopin, M. Tchernycheva, C. Durand, J. Eymery, M-Plane Core–Shell InGa_N/Ga_N Multiple-Quantum-Wells on Ga_N Wires for Electroluminescent Devices, *Nano Lett*. 11 (2011) 4839–4845. <https://doi.org/10.1021/nl202686n>.
- [4] V. Grenier, S. Finot, L. Valera, J. Eymery, G. Jacopin, C. Durand, UV-A to UV-B electroluminescence of core-shell Ga_N/AlGa_N wire heterostructures, *Applied Physics Letters*. 121 (2022) 131102. <https://doi.org/10.1063/5.0101591>.
- [5] V. Grenier, S. Finot, B. Gayral, C. Bougerol, G. Jacopin, J. Eymery, C. Durand, Toward Crack-Free Core–Shell Ga_N/AlGa_N Quantum Wells, *Crystal Growth & Design*. 21 (2021) 6504–6511. <https://doi.org/10.1021/acs.cgd.1c00943>.
- [6] C. Durand, C. Bougerol, J.-F. Carlin, G. Rossbach, F. Godel, J. Eymery, P.-H. Jouneau, A. Mukhtarova, R. Butté, N. Grandjean, *M*-Plane Ga_N/InAl_N Multiple Quantum Wells in Core–Shell Wire Structure for UV Emission, *ACS Photonics*. 1 (2014) 38–46. <https://doi.org/10.1021/ph400031x>.
- [7] M. Djavid, Z. Mi, Enhancing the light extraction efficiency of AlGa_N deep ultraviolet light emitting diodes by using nanowire structures, *Appl. Phys. Lett*. 108 (2016) 051102. <https://doi.org/10.1063/1.4941239>.
- [8] T. Onuma, H. Amaike, M. Kubota, K. Okamoto, H. Ohta, J. Ichihara, H. Takasu, S.F. Chichibu, Quantum-confined Stark effects in the *m*-plane In_{0.15}Ga_{0.85}N/Ga_N multiple quantum well blue light-emitting diode fabricated on low defect density freestanding Ga_N substrate, *Appl. Phys. Lett*. 91 (2007) 181903. <https://doi.org/10.1063/1.2802042>.
- [9] M. Yoshizawa, A. Kikuchi, M. Mori, N.F. Nobuhiko Fujita, K.K. Katsumi Kishino, Growth of Self-Organized Ga_N Nanostructures on Al₂ O₃ (0001) by RF-Radical Source Molecular Beam Epitaxy, *Jpn. J. Appl. Phys*. 36 (1997) L459. <https://doi.org/10.1143/JJAP.36.L459>.
- [10] G.W. Pickrell, A.M. Armstrong, A.A. Allerman, M.H. Crawford, C.E. Glaser, J. Kempisty, V.M. Abate, Investigation of dry-etch-induced defects in >600 V regrown, vertical, Ga_N, p-n diodes using deep-level optical spectroscopy, *Journal of Applied Physics*. 126 (2019) 145703. <https://doi.org/10.1063/1.5110521>.
- [11] K. Zhang, T. Takahashi, D. Ohori, G. Cong, K. Endo, N. Kumagai, S. Samukawa, M. Shimizu, X. Wang, High-quality nanodisk of InGa_N/Ga_N MQWs fabricated by neutral-beam-etching and Ga_N regrowth: towards directional micro-LED in top-down structure, *Semicond. Sci. Technol*. 35 (2020) 075001. <https://doi.org/10.1088/1361-6641/ab8539>.
- [12] L. Jaloustre, V. Ackermann, S.S.D. Mello, S. Labau, C. Petit-Etienne, E. Pargon, Preferential crystal orientation etching of Ga_N nanopillars in Cl₂ plasma, *Materials Science in Semiconductor Processing*. 165 (2023) 107654. <https://doi.org/10.1016/j.mssp.2023.107654>.
- [13] D.A. Stocker, E.F. Schubert, J.M. Redwing, Crystallographic wet chemical etching of Ga_N, *Appl. Phys. Lett*. 73 (1998) 2654–2656. <https://doi.org/10.1063/1.122543>.
- [14] M. Itoh, T. Kinoshita, C. Koike, M. Takeuchi, K. Kawasaki, Y. Aoyagi, Straight and Smooth Etching of Ga_N (1-100) Plane by Combination of Reactive Ion Etching and KOH Wet Etching Techniques, *Jpn. J. Appl. Phys*. 45 (2006) 3988–3991. <https://doi.org/10.1143/JJAP.45.3988>.
- [15] K.H. Baik, H.-Y. Song, S.-M. Hwang, Y. Jung, J. Ahn, J. Kim, Etched Surface Morphology of Heteroepitaxial Nonpolar (11-20) and Semipolar (11-22) Ga_N Films by Photoenhanced Chemical Wet Etching, *J. Electrochem. Soc*. 158 (2011) D196–D199. <https://doi.org/10.1149/1.3544916>.

- [16] D. Li, M. Sumiya, S. Fuke, D. Yang, D. Que, Y. Suzuki, Y. Fukuda, Selective etching of GaN polar surface in potassium hydroxide solution studied by x-ray photoelectron spectroscopy, *Journal of Applied Physics*. 90 (2001) 4219–4223. <https://doi.org/10.1063/1.1402966>.
- [17] Y.-Y. Lai, S.-C. Hsu, H.-S. Chang, Y.S. Wu, C.-H. Chen, L.-Y. Chen, Y.-J. Cheng, The study of wet etching on GaN surface by potassium hydroxide solution, *Research on Chemical Intermediates*. 43 (2017) 3563–3572. <https://doi.org/10.1007/s11164-016-2430-1>.
- [18] F. Yu, S. Yao, F. Römer, B. Witzigmann, T. Schimpke, M. Strassburg, A. Bakin, H.W. Schumacher, E. Peiner, H.S. Wasisto, A. Waag, GaN nanowire arrays with nonpolar sidewalls for vertically integrated field-effect transistors, *Nanotechnology*. 28 (2017) 095206. <https://doi.org/10.1088/1361-6528/aa57b6>.
- [19] M.A. Gosálvez, K. Sato, A.S. Foster, R.M. Nieminen, H. Tanaka, An atomistic introduction to anisotropic etching, *J. Micromech. Microeng.* 17 (2007) S1–S26. <https://doi.org/10.1088/0960-1317/17/4/S01>.
- [20] M.A. Gosálvez, Yan Xing, K. Sato, Analytical Solution of the Continuous Cellular Automaton for Anisotropic Etching, *J. Microelectromech. Syst.* 17 (2008) 410–431. <https://doi.org/10.1109/JMEMS.2008.916339>.
- [21] M. Fouchier, E. Pargon, Atomic force microscopy study of photoresist sidewall smoothing and line edge roughness transfer during gate patterning, *J. Micro/Nanolith. MEMS MOEMS*. 12 (2013) 041308. <https://doi.org/10.1117/1.JMM.12.4.041308>.
- [22] D.L. Goldfarb, A.P. Mahorowala, G.M. Gallatin, K.E. Petrillo, K. Temple, M. Angelopoulos, S. Rasgon, H.H. Sawin, S.D. Allen, M.C. Lawson, R.W. Kwong, Effect of thin-film imaging on line edge roughness transfer to underlayers during etch processes, *Journal of Vacuum Science & Technology B: Microelectronics and Nanometer Structures Processing, Measurement, and Phenomena*. 22 (2004) 647–653. <https://doi.org/10.1116/1.1667513>.
- [23] V. Constantoudis, G. Kokkoris, P. Xydi, G.P. Patsis, E. Gogolides, Modeling of line edge roughness transfer during plasma etching, *Microelectronic Engineering*. 86 (2009) 968–970. <https://doi.org/10.1016/j.mee.2009.01.040>.
- [24] G. Kokkoris, V. Constantoudis, E. Gogolides, Nanoscale Roughness Effects at the Interface of Lithography and Plasma Etching: Modeling of Line-Edge-Roughness Transfer During Plasma Etching, *IEEE Trans. Plasma Sci.* 37 (2009) 1705–1714. <https://doi.org/10.1109/TPS.2009.2024117>.
- [25] J. He, M. Feng, Y. Zhong, J. Wang, R. Zhou, H. Gao, Y. Zhou, Q. Sun, J. Liu, Y. Huang, S. Zhang, H. Wang, M. Ikeda, H. Yang, On-wafer fabrication of cavity mirrors for InGaN-based laser diode grown on Si, *Sci Rep.* 8 (2018) 7922. <https://doi.org/10.1038/s41598-018-26305-8>.
- [26] Y. Jung, K.H. Baik, M.A. Mastro, J.K. Hite, C.R. Eddy, J. Kim, Chemical etching behaviors of semipolar (11-22) and nonpolar (11-20) gallium nitride films, *Phys. Chem. Chem. Phys.* 16 (2014) 15780. <https://doi.org/10.1039/C4CP02303J>.